DOI 10.5162/IMCS2012/P1.7.4

Preparation of In_2O_3/TiO_2 composite nanofibers by electrospinning and their application as a HCHO gas sensor with two operating conditions

*Pengpeng Chen[1], Jing Wang[1, *], Pengjun Yao[1, 2]*
[1] School of Electronic Science and Technology, Dalian University of Technology, Dalian 116023,China
[2] School of Educational Technology, Shenyang Normal University, Shenyang 110034, China
** Corresponding author: wangjing@dlut.edu.cn*

Abstract:
In this paper In_2O_3 and TiO_2 porous nanofibers were respectively synthesized by electrospinning method and characterized with XRD, SEM and TEM. The average grain sizes of In_2O_3 and TiO_2 nanofibers are 32 nm and 40 nm, respectively. As-prepared In_2O_3 and TiO_2 nanofibers were mixed in 1:1 molar ratio to fabricate formaldehyde (HCHO) gas sensor. The gas-sensing properties of the composite In_2O_3/TiO_2 sensor were measured at two operating conditions: heating and UV-LED illumination, respectively. The sensor exhibited high sensitivity and good selectivity to HCHO vapor at both operating conditions.

Key words: Gas sensor, In_2O_3, TiO_2, Heating, UV-LED

1. Introduction

One dimensional (1D) metal-oxide semiconductors (MOS) nanostructures with high surface to volume ratio and effective electron transport have been gained considerable attention in fabrication of miniature gas sensors [1]. Among varieties of methods for synthesizing 1D nanostructures, electrospinning is a simple, effective, low-cost and powerful approach to prepare 1D nanomaterials including polymer, inorganic and composite [2]. Normally, a MOS gas sensor worked at an operating condition of high temperature and hardly worked at room temperature or in complex gas environments [3]. In_2O_3 (band gap=3.55–3.75 eV) and TiO_2 (band gap=3.0–3.2 eV) have been widely used in solar cells, transparent conductors, and gas sensors because of well optical and electronic characters. In this report, a composite nanofibers In_2O_3/TiO_2 gas sensor was fabricated and worked at two operating conditions: heating (high temperature) and UV-LED irradiation, respectively.

2. Experiment

First, 382 mg $In(NO_3)_3 \cdot 4.5H_2O$ power was dissolved in 2.5 ml DMF and 3.0 ml ethanol under vigorous stirring for 2 h. Then 382 mg PVP was added to the above solution and stirred for 6 h to transparent PVP/ $In(NO_3)_3 \cdot 4.5H_2O$ solution for electrospinning [2]. The as-electrospun PVP/$In(NO_3)_3 \cdot 4.5H_2O$ composite nanofibers were annealed in air at 500˚C to obtain In_2O_3 nanofibers. In the same way, TiO_2 nanofibers were prepared by electrospinning and then annealed in air at 600˚C, respectively. The as-prepared In_2O_3 and TiO_2 nanofibers were mixed in 1:1 molar ratio and then were fabricated to a gas sensor. Two operating conditions for the sensor were provided: A Ni-Cr heating wire with resistance 30 Ω as a heater was inserted through a ceramic tube to provide an operating temperature, as shown in Fig. 1 (a); and a 365 nm UV-LED were placed both under and above the tube to make the gas sensor operate without heating (Fig. 1 (b)). The voltage applied on the Ni-Cr heating wire and UV-LED was 3.0V and 3.6V, respectively.

(a) Ceramic tube for heating (b) UV-LED

Fig. 1 The structure graph of the gas sensor with two operating conditions

The gas-sensing properties of the gas sensor based on In_2O_3/TiO_2 composite nanofibers were measured using a static state gas-sensing test system [4]. The Measurement temperature (18◦C±2◦C) and humidity (~25%±5%RH) can be well controlled during the measurement. The sensors were first irradiated with UV-LED or first heated by Ni-Cr heating wire for 30 min to stabilize the electrical properties of the sensor [5]. The gas response (S) was defined as a ratio of the electrical resistance of the sensor in air (R_a) to that in target gas (R_g): $S=R_a/R_g$. The time taken by the sensor to achieve 90% of the total resistance change was defined as the response time in the case of adsorption or the recovery time in the case of desorption [6].

3. Result and discussion

3.1 Characterization of In_2O_3 and TiO_2 nanofibers

Fig. 2 shows the XRD patterns of the In_2O_3 and TiO_2 nanofibers. The stronger and sharper diffraction peaks in curves (a) and (b) show that the In_2O_3 and TiO_2 nanofibers have a high degree of crystallization. Meanwhile, Fig. 2 (b) shows that forms of anatase (the solid square symbol) and rutile (the hollow square symbol) for TiO_2 nanofibers occurred, which belong to the tetragonal crystal system. And we can see that the peaks of anatase TiO_2 (marked in red) were sharper than those of rutile TiO_2(marked in blue). According to the Scherrer equation, the average sizes of In_2O_3 nanofibers were 32 nm and that of the TiO_2 were 40 nm, respectively.

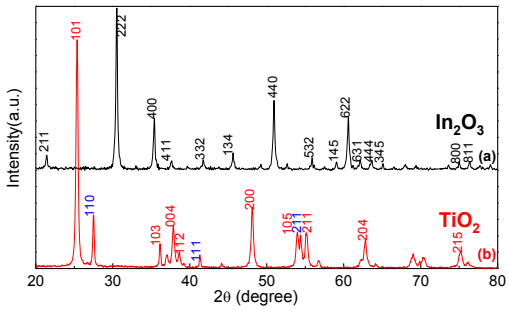

Fig.2. The XRD patterns of the In_2O_3 and TiO_2 nanofibers

The general morphologies of In_2O_3 and TiO_2 nanofibers were studied with scan electronic microscope (SEM) and transmission electronic microscope (TEM) as shown in Fig. 3 (a～d), respectively. Fig. 3 (a) and (c) obviously show that the diameters of In_2O_3 and TiO_2 were around 120 nm and 80 nm after calcination. Meanwhile, after calcination the surface of In_2O_3 and TiO_2 nanofibers become rough and the lengh of TiO_2 nanofibers have been mildly broken because of the decomposition of PVP. The TEM images of a single In_2O_3 and a single TiO_2 nanofiber in Fig. 3 (b) and (d) show that the as-prepared nanofibers with nano hierarchical structure are indeed composed of many interconnected grains of around 32 nm and 40 nm, respectively. From Fig. 3 (b) and (c) we can see that the In_2O_3 nanofibers represent well mesoporous morphology which can enhance the gas adsorption.

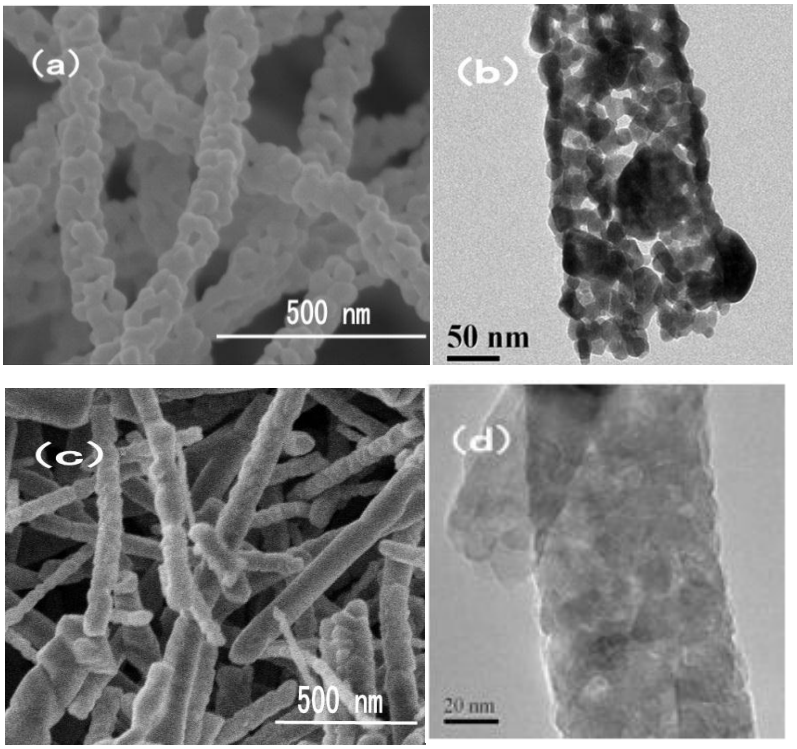

Fig.3. SEM and TEM images of In_2O_3 (a, b) and TiO_2 (c, d) nanofibers, respectively

3.2 Gas sensing properties of the sensors

Here the HCHO sensing properties of the sensors based on In_2O_3 doped with TiO_2 nanorods were tested under heating condition and UV-LED light at room temperature, respectively. The measurement showed that the optimum working temperature of the gas sensor was 280˚C at heating condition and the optimum working voltage connected with UV-LED was 3.6 V.

Fig.4 (a) and (b) show the dependence of response of the In_2O_3/TiO_2 sensors on the concentration of HCHO at two operating conditions, respectively. We can see from Fig.4 (a) that the sensors have higher response in low HCHO concentration range (1-10 ppm) at heating condition. Though the corresponding response of the sensors worked at UV-LED condition seems much smaller than at heating condition when the concentration of HCHO in the range of 10-1000 ppm, the sensors supplied by UV-LED light energy can work at room temperature. As shown in Fig.4 (a) and (b), there is a well linear correlation between the response of the sensors and the concentration of HCHO at the two operating conditions.

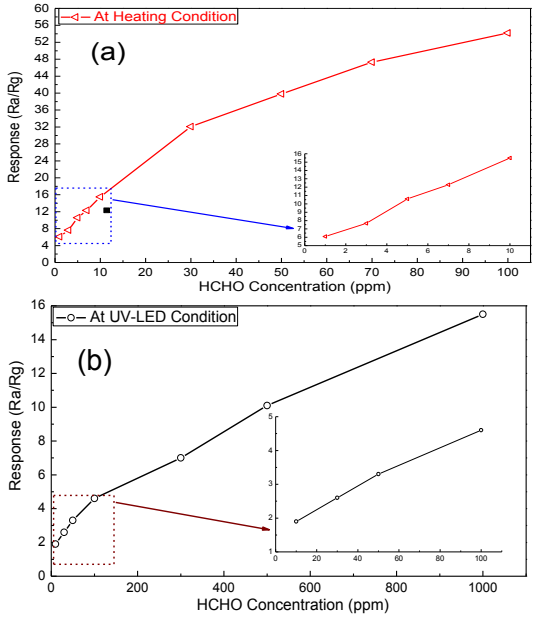

Fig. 4. Response of the In_2O_3/TiO_2 based sensors to different concentration of HCHO at two operating conditions (a) heating, (b) UV-LED illumination

The responses at the two operating conditions change with time under different HCHO gas concentrations were shown in Fig.5 (a) and (b), respectively. As shown in the insets in Fig.5 (a) and (b), the response/recovery time of the sensors were 60 s and 80 s to 1 ppm HCHO at heating condition, 170 s and 320 s to 100 ppm HCHO at UV-LED condition, respectively.

The selectivity of the sensors to formaldehyde, ethanol, methanol, toluene, acetone and ammonia were also analyzed as shown in Fig. 6. The results indicated that the sensors to 10 ppm different gases exhibited a significantly higher response to formaldehyde than to other gases at the heating temperature of 280˚C. And to 100 ppm different gases, the sensors also exhibited well sensitive to formaldehyde and less sensitive to other gases at room temperature under UV-LED light illumination.

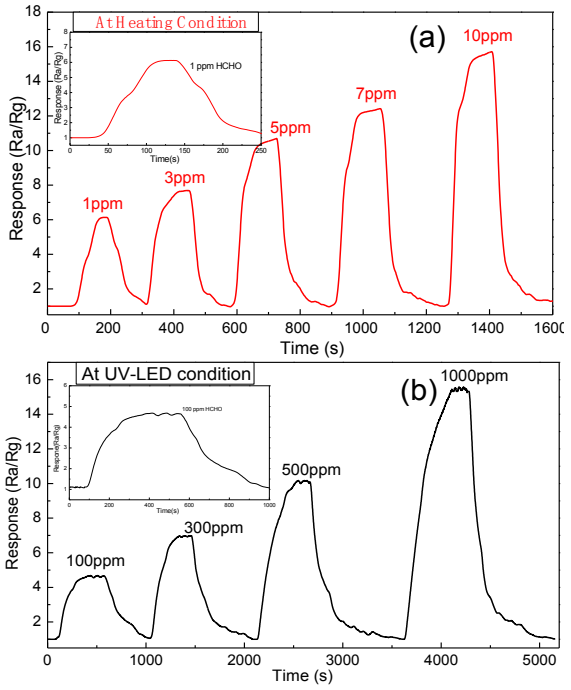

Fig. 5. Responses change with time to different concentration of HCHO at the two operating conditions (a) heating, (b) UV-LED illumination. The inset in (a) and (b) is the response/recovery curve to 1ppm HCHO at heating condition100 ppm HCHO at UV-LED condition, respectively.

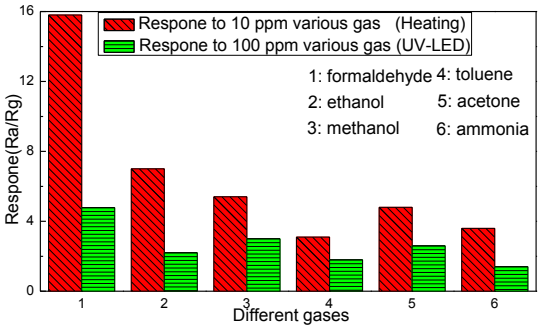

Fig. 6. The selectivity of the In_2O_3/TiO_2 based sensors at the two operating conditions

3.3 Mechanisms of gas sensing at UV-LED condition

The mechanisms of gas sensing of In_2O_3/TiO_2 composite fibers at the heating conditions was explained as Y.D. W reported [7]. The mechanisms of gas sensing under UV-LED illumination is discussed as fellows. A type of

heterojunction can be easily formed in the In_2O_3/TiO_2 interface because of the different band gap between In_2O_3 (3.55–3.75 eV) and TiO_2 (3.0–3.2 eV). The electrons at the valence band of TiO_2 absorbed the UV light and will transfer from the conduction band of TiO_2 to that of In_2O_3. Conversely, the hole will transfer from the valence band of In_2O_3 to that of TiO_2 [8]. These photogenerated electron-hole pairs as Eq. (1) will migrate to the surface of the semiconductor material by the action of the build-in electric field. First, the sensors were operated in ambient air, oxygen molecules will trap the electron on the surface of the semiconductor materials and turn to oxygen ions O_2^- as Eq. (2) [9-10]. During the process of O_2 chemisorption balance on the surface of the semiconductor materials and recombination of part of photogenerated electron-hole pairs, the resistance of the sensor increases because of the decrease of charge carriers. When the sensors exposure to HCHO gas UV-LED illumination, the oxygen ions O_2^- generated as Eq. (2) will be trapped by HCHO, and the reaction occurs as Eq. (3) [7]. Then the recombination between the photogenerated electron and HCHO gas molecule will reduce the interface potential barrier and depletion-layer width. Thus, the resistance of the sensor decreases with the increase of charge carriers concentration caused by released electron as Eq. (3) and the increase tunneling probability of carrier transport.

$$TiO_2 + In_2O_3 \xrightarrow{hv} e^- + h^+ \quad (1)$$

$$O_{2\,gas} + 2e^- \leftrightarrow O_{ads}{}^{2-} \quad (2)$$

$$HCHO_{(ads)} + 2O_{(ads)}{}^{2-} \rightarrow CO_2 + H_2O + 4e^- \quad (3)$$

4. Conclusion

In_2O_3 and TiO_2 porous nanofibers were synthesized by using electrospinning method, respectively. The HCHO gas sensors based on In_2O_3/TiO_2 composite nanofibers have a higher response to low concentration of formaldehyde (1 ppm-10 ppm) at the heating temperature of 280°C, and have a well linear relation between the response and the concentration of formaldehyde (10 ppm-1000ppm) at UV-LED condition. Thus, the sensors can measure formaldehyde vapor in a concentration range of 1-1000 ppm. Furthermore, the sensors exhibited rapid response/recovery time, good selectivity both at heating and UV-LED irradiation conditions. We can choose the optimum operating conditions according to the testing environment and test requirements.

Acknowledgements

Authors thank to The National Natural Science Foundation of China for financial support (61176068, 61131004, 61001054).

References

[1] A. Kolmakov, M. Moskovits, Chemical sensing and catalysis by one-dimensional metal-oxide nanostructures, Annu.Rev.Mater.34(2004)151-180; doi: 1146/annurev.matsci.34.040203.112141

[2] W. Zheng, X.F. Lu, W. Wang, Z.Y. Li, H.N. Zhang, Y. Wang, Z.J. Wang, C. Wang, A highly sensitive and fast-responding sensor based on electrospun In_2O_3 nanofibers, Sensors and Actuators B ,142 (2009) 61-65; doi: 10.1016/j.snb.2009.07.031

[3] Sang Kyoo Lim, Sung-Ho Hwang, Daeic Chang, Soonhyun Kim, Preparation of mesoporous I_{n2O3} nanofibers by electrospinning and their application as a CO gas sensor, Sensors and Actuators B ,149 (2010) 28-33; doi: 10.1016/j.snb.2010.06.039

[4] G.Y. Lu, J. Xu, J.B. Sun, Y.S. Yu, Y.Q. Zhang ,F.M. Liu, UV-Enhanced Room Temperature NO_2 Sensor Using ZnO Nanorods Modified with SnO_2 Nanoparticles, Sensors and Actuators B,162 (2012) 82- 88; doi: 10.1016/j.snb.2011.12.039

[5] V.E. Henrich, The surfaces of metal-oxides, Rep. Prog. Phys., 48 (1985) 1481-1541; doi: 10.1088/0034-4885/48/11/001

[6] R.L. Vander Wal, G.W. Hunter, J.C. Xu, M.J. Kulis, G.M. Berger, T.M. Ticich, Metal-oxide nanostructure and gas-sensing performance, Sensors and Actuators B, 138 (2009) 113-119; doi: 10.1016/j.snb.2009.02.020

[7] T. Chen, Z.L. Zhou, Y.D. Wang, Effects of calcining temperature on the phase structure and the formaldehyde gas sensing properties of CdO-mixed In_2O_3, Sensors and Actuators B, 135 (2008) 219-223; doi: 10.1016/j.snb.2008.08.013

[8] J. Peral, X. Domenech, D.F. Ollis, Heterogeneous photocatalysis for purification, decontamination and deodorization of air, Chem. Technol. Biotechnol. 70 (1997) 117-140; doi: 10.1002/(SICI)1097-4660(199710)

[9] N. Barsan, U. Weimar, Conduction model of metal oxide gas sensors, J. Electroceram.7 (2001) 143-167; doi: 10.1023/A:1014405811371

[10] K. Anothainart, M. Burgmair, A. Karthigeyan, M. Zimmer, I. Eisele, Light enhanced NO_2 gas sensing with tin oxide at room temperature: conductance and work function measurements, Sens. Actuators B: Chem. 93 (2003) 580-584; doi:10.1016/S0925-4005(03)00220-X